DOI : 10.1016/j.jweia.2020.104160

Effects of wind speed and atmospheric stability on the air pollution reduction rate induced by noise barriers

Nicolas Reiminger[1,2*], Xavier Jurado[1,2], José Vazquez[2], Cédric Wemmert[2], Nadège Blond[3], Matthieu Dufresne[1], Jonathan Wertel[1]

[1]*AIR&D, 67000, Strasbourg, France*
[2]*ICUBE Laboratory, CNRS/University of Strasbourg, 67000, Strasbourg, France*
[3]*LIVE Laboratory, CNRS/University of Strasbourg, 67000, Strasbourg, France*
[*]*Corresponding author: Tel. +33 (0)6 31 26 75 88, Mail. nreiminger@air-d.fr*

Please cite this paper as : Reiminger, N., Jurado, X., Vazquez, J., Wemmert, C., Blond, N., Dufresne, M., Wertel, J., 2020. Effects of wind speed and atmospheric stability on the air pollution reduction rate induced by noise barriers. Journal of Wind Engineering and Industrial Aerodynamics 200, 104160. https://doi.org/10.1016/j.jweia.2020.104160

ABSTRACT

People around the world increasingly live in urban areas where traffic-related emissions can reach high levels, especially near heavy-traffic roads. It is therefore necessary to find short-term measures to limit the exposure of this population and noise barriers have shown great potential for achieving this. Nevertheless, further work is needed to better understand how they can act on pollution reduction. To do this, a Reynolds-Averaged Navier-Stokes model that takes into account thermal effects is used to study the effects of wind speed and atmospheric stability on the concentration reduction rates (*CRR*) induced by noise barriers. This study shows that the *CRR* behind the barriers may depend on both wind and thermal conditions. Although only the wind direction, and not the wind speed, has an impact on *CRR* in a neutral atmosphere, this parameter can be changed by both wind speed and thermal variations in non-neutral atmospheres. Stable cases lead to a higher *CRR* compared to unstable cases, while the neutral case gives intermediate results. Finally, it is shown that the variation of *CRR* is negligible for Richardson numbers ranging from -0.50 to 0.17.

Keywords: Computational fluid dynamics, Noise barrier, Air pollution, Wind speed, Thermal stratification

DOI : 10.1016/j.jweia.2020.104160

Highlights

- Wind speed does not change concentration reduction rates (*CRR*) for neutral cases.
- For neutral cases, perpendicular winds lead to the lowest *CRR.*
- The global *CRR* decreases as a function of height and distance from the barriers.
- *CRRs* are higher for stable cases ($Ri > 0$) and lower for unstable cases ($Ri < 0$).
- *CRRs* remain unchanged for a given Richardson number ranging from -0.50 to 0.17.

DOI : 10.1016/j.jweia.2020.104160

1. Introduction

Nowadays, more than one in two people live in urban areas with 82% in the United States and 74% in Europe, and this percentage will continue growing to reach 68% worldwide in 2050 (United Nations, 2019). Traffic-related emissions can reach high levels in such areas, particularly near heavy-traffic roads. Concentrations of air pollutants such as nitrogen dioxide (NO_2) and particulate matter (PM) can reach high values in the vicinity of this kind of road and lead to several diseases (Anderson et al., 2012; Kagawa, 1985; Kim et al., 2015). In addition, it has been shown that people living near these roads are more likely to be at risk (Chen et al., 2017; Finkelstein et al., 2004; Petters et al., 2004). In Europe, emissions and therefore concentrations of air pollutants are expected to decrease in the future as air quality regulations increase and actions are taken (European Commission, 2013). Nevertheless, it will take time to achieve a significant decrease and, in the meantime, many people will still live in areas where air quality is poor. It is now necessary to find ways to limit exposure to air pollution for people living near busy roads and to better understand solutions that have already been found, like noise barriers.

Noise barriers are civil engineering elements located along roadways and designed to protect inhabitants from noise pollution. These elements, often placed between heavy-traffic roads and residences, also have a beneficial impact on air quality. Indeed, several authors have investigated the efficiency of noise barriers in reducing atmospheric pollutant concentrations behind the barriers using in-field (Baldauf et al., 2008, 2016; Finn et al., 2010; Hagler et al., 2012; Lee et al., 2018; Ning et al., 2010), wind tunnel (Heist et al., 2009) measurements and numerical models (Bowker et al., 2007; Hagler et al., 2011; Schulte et al., 2014). Some authors have studied the effects of barrier heights and distances on pollution reduction (Amini et al., 2018; Gong and Wang, 2018). Other authors have studied the effects of barrier shapes and locations on improving the reduction of atmospheric pollutants (Brechler and Fuka, 2014; Enayati Ahangar et al., 2017; Wang and Wang, 2019). However, although some of these works have been performed by considering different atmospheric stabilities, knowledge is lacking on how the combination of wind conditions and thermal effects can affect pollutant reductions behind barriers. Further work is thus required in this direction.

The aim of this work is to study the combined effects of wind and thermal effects on the reduction of pollutant concentrations behind the noise barrier. The scope of the study is limited to the study of the effects of the noise barriers and doesn't include the possible effects of

DOI : 10.1016/j.jweia.2020.104160

buildings before and after the barriers. More specifically, computational fluid dynamics (CFD) simulations are used to assess the evolution of the concentration reduction rate behind noise barriers for several wind speeds and atmospheric stabilities, ranging from very unstable to stable conditions, including all the intermediate conditions (unstable, slightly unstable, neutral and slightly stable). The two key parameters of this study are defined and described in Section 2. The numerical model, including the governing equations, boundary conditions and model validation used in this work, is presented in Section 3. The results of the study are presented in Section 4, after which these results are discussed in Section 5.

2. Description of the study

This paper examines the impact of wind speed and atmospheric stability on the reduction of downwind air pollution induced by the presence of noise barriers. It is therefore necessary to define two recurring parameters: the Richardson number and the concentration reduction rate.

The thermal effects can be quantified using the Richardson number noted Ri. The corresponding equation taken from (Woodward, 1998) is given in (1).

$$Ri = \frac{gH}{{U_H}^2}\frac{(T_H - T_w)}{T_{air}} \qquad (1)$$

where g is the gravitational acceleration [m.s^{-2}], H is the noise barrier height [m], U_H is the reference velocity (which is the velocity at $z = H$ in this study) [m.s^{-1}], T_{air} is the ambient temperature [K], T_H is mean air temperature at $z = H$ [K], and T_w is the surface temperature of the heated ground [K]. The difference $T_H - T_w$ will be noted ΔT in the following.

The Richardson number is also an indicator of atmospheric stability: $Ri = 0$ corresponds to isothermal (neutral) cases, $Ri < 0$ corresponds to unstable cases, and $Ri > 0$ to stable cases. A better discretization of atmospheric stability, related to Pasquill's stability classes, also exists (Woodward, 1998) and is summarized in Table 1.

Table 1. Atmospheric stability correlated with the Richardson number (Woodward, 1998).

Atmospheric stability	Richardson number
Very unstable	$Ri < -0.86$
Unstable	$-0.86 \leq Ri < -0.37$
Slightly unstable	$-0.37 \leq Ri < -0.10$
Neutral	$-0.10 \leq Ri < 0.053$
Slightly stable	$0.053 \leq Ri < 0.134$
Stable	$0.134 \leq Ri$

DOI : 10.1016/j.jweia.2020.104160

The reduction of the pollution behind the noise barriers compared to an area without these barriers is quantified using an indicator called concentration reduction rate (CRR) given in (2).

$$CRR\ (\%) = \left(1 - \frac{C_{nb}}{C_{ref}}\right) \times 100 \qquad (2)$$

where C_{nb} is the concentration with a noise barrier [kg.m^{-3}] and C_{ref} is the reference concentration corresponding to the same case but without noise barriers [kg.m^{-3}].

The CRR provides information on both the positive and negative impact of noise barriers ($CRR > 0$ means that noise barriers reduce downwind pollution; $CRR < 0$ means that noise barriers increase downwind pollution) and their effectiveness (CRR = 40% means that the concentration behind noise barriers is reduced by 40% compared to the same case without them).

3. Numerical model

3.1. Governing equations

Simulations were performed using the *buoyantPimpleFoam* solver from OpenFOAM 6.0. This transient solver is able to resolve Navier-Stokes equations for buoyant and turbulent flows of compressible fluids including the effects of forced convection (induced by the wind) and natural convection (induced by heat transfers).

A Reynolds-averaged Navier-Stokes (RANS) methodology was used to resolve the equations. When using this methodology, a new term called Reynolds stress tensor appear and it is necessary to choose a turbulence model to resolve it. The RNG k-ε turbulence model proposed by Yakhot et al. (1992) has been selected because it gives significant improvements compared to the standard turbulence model for recirculatory flows (Papageorgakis and Assanis, 1999), whereas anisotropic models such as the Reynolds Stress Model (RSM) may not improve the results (Koutsourakis et al., 2012) for a higher calculation cost and more calculation instabilities.

The corresponding continuity (3), momentum (4) and energy (5) equations are given below:

$$\frac{\partial \rho}{\partial t} + \nabla.(\rho u) = 0 \qquad (3)$$

$$\rho\left(\frac{\partial u}{\partial t} + u.\nabla u\right) = -\nabla p + \nabla.\ \left(2\mu_{eff} D(u)\right) - \nabla\left(\frac{2}{3}\mu_{eff}(\nabla.u)\right) + \rho g \qquad (4)$$

DOI : 10.1016/j.jweia.2020.104160

$$\frac{\partial \rho e}{\partial t} + \nabla.(\rho u e) + \frac{\partial \rho K}{\partial t} + \nabla.(\rho u K) + \nabla.(up) = \nabla.\left(\alpha_{eff} \nabla e\right) + \rho g.u \qquad (5)$$

$$D(u) = \frac{1}{2}[\nabla u + (\nabla u)^T] \qquad (6)$$

$$K \equiv |u|^2/2 \qquad (7)$$

where u is the velocity [m.s^{-1}], p the pressure [kg.m^{-1}.s^{-2}], ρ the density [kg.m^{-3}], e the thermal energy [m^2.s^{-2}], $D(u)$ the rate of strain tensor given in (6), K the kinetic energy given in (7) [m^2.s^{-2}], g the gravitational acceleration [m.s^{-2}], μ_{eff} the effective viscosity defined as the sum of molecular and turbulent viscosity [kg.m^{-1}.s^{-1}] and α_{eff} the effective thermal diffusivity defined as the sum of laminar and turbulent thermal diffusivities [kg.m^{-1}.s^{-1}].

No chemical reactions are considered in this study. Thus, the equation governing passive scalar transport (8) has been added to the solver. This advection-diffusion equation is given below:

$$\frac{\partial C}{\partial t} + \nabla.(uC) - \nabla.\left[\left(D_m + \frac{\nu_t}{Sc_t}\right)\nabla C\right] = E \qquad (8)$$

where C is the pollutant concentration [kg.m^{-3}], D_m is the molecular diffusion coefficient [m^2.s^{-1}], ν_t the turbulent diffusivity [m^2.s^{-1}], Sc_t the turbulent Schmidt number [-] and E the volumetric source term of the pollutants (emissions) [kg.m^{-3}.s^{-1}].

Each simulation was performed using second order schemes for all the gradient, divergent and Laplacian terms. The streamwise velocity U and the pollutant concentration C were monitored for several locations behind the downwind noise barrier and the results were checked to ensure that each simulation has converged. At the end of the simulations, all the residuals were under 10^{-5}.

3.2. Computational domain and boundary conditions

This study focuses on the concentration reduction rates induced by the presence of noise barriers. Thus, to quantify this reduction, two distinct cases have to be considered in terms of computational domain: a case with noise barriers and a case without them. Fig. 1 shows a sketch of the computational domain and the boundary conditions used for the case with noise barriers. The second case is strictly the same but without the noise barriers.

DOI : 10.1016/j.jweia.2020.104160

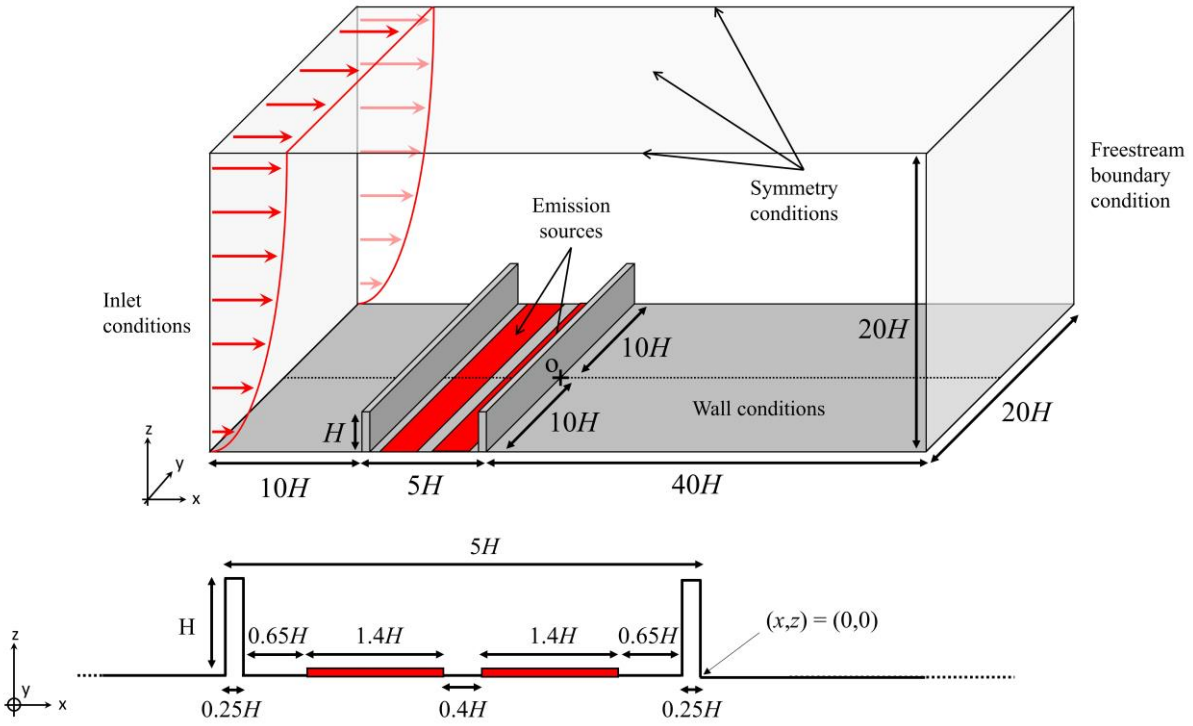

Fig.1. Sketch of the computational domain with H = 5 m.

The recommendations given by Franke et al. (2007) were followed concerning the boundary conditions and domain size. The inlet boundary is localized 10H before the upwind noise barrier where velocity, turbulence and temperature profiles are specified using a perpendicular wind direction, unless otherwise stated. The outlet boundary is placed 40H behind the downwind noise barrier with a freestream condition to allow the flow to fully develop. Symmetry conditions are applied for the upper and lateral limits, with the top of the calculation domain placed 20H from the ground and the lateral limits located 20H from each other. No-slip conditions are applied to any other boundaries including the ground and the two noise barriers, where the temperature can be specified to simulate stable and unstable cases. Finally, traffic exhausts are modeled by two volumetric sources along the y-direction, with a width of 1.4H each, and over one mesh height (0.25 m) where an emission source term is added in the pollutant transport equation. A mass flow rate of 100 g/s is used for all the simulations performed. Further information can be found in Table 2.

DOI : 10.1016/j.jweia.2020.104160

Table 2. Summary of the boundary conditions.

Inlet	Velocity and turbulence profiles are calculated according to Richards and Hoxey (1993) and Richards and Norris (2011): $U = \frac{u_*}{\kappa} ln\left(\frac{z}{z_0}\right)$ (9) $k = \frac{{u_*}^2}{\sqrt{C_\mu}}$ (10) $\varepsilon = \frac{{u_*}^3}{\kappa.z}$ (11) with U the wind velocity, k the turbulent kinetic energy (TKE), ε the dissipation of TKE, u_* the friction velocity, κ the von Kármán constant taken to 0.41, z the altitude, z_0 the roughness height taken as 0.5 m, and C_μ a CFD constant taken as 0.085. Fixed temperature: T_{air} = 293 K.
Outlet	Freestream outlet.
Top	Symmetry plane.
Lateral surfaces	Symmetry plane.
Ground and noise barriers surfaces	No-slip condition (U = 0 m/s). Fixed temperature (T_w) depending on the case studied.
Emission	Surface source with emission rate q_m = 100 g/s.

The most part of the simulations have been carried out considering à perpendicular incident wind angle (90°) with respect to the noise barrier, but some simulations were also performed with a 60° incident angle. The boundary conditions were the same in both configurations and Fig. 2. presents how the incidence angle is defined.

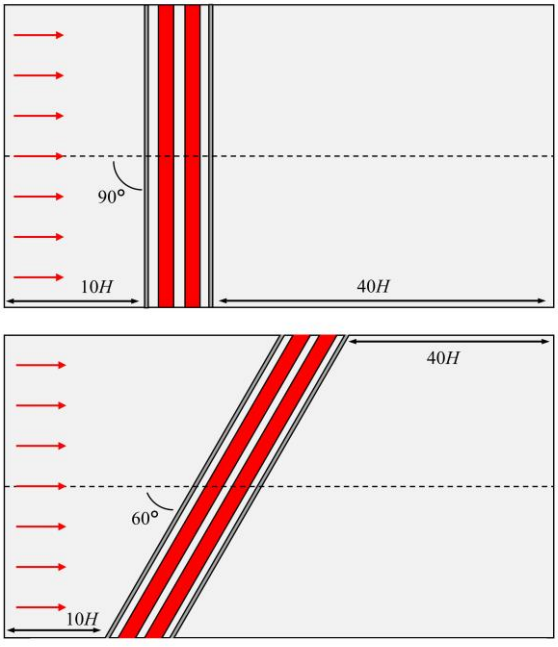

Fig.2. Definition of the wind incidence angle.

DOI : 10.1016/j.jweia.2020.104160

Mesh sensitivity tests were carried out to ensure that the results are fully independent of mesh size. Successive simulations were performed with different mesh sizes and the Grid Convergence Index (*GCI*) methodology (Roache, 1994) was used to assess the mesh-related errors on both the flow field and the concentration field. Mean *GCIs* of 2% and 1% were obtained for flow and concentration fields, respectively, when comparing the results from mesh sizes of 0.5 m and 0.25 m. Thus, a mesh size of 0.5 m was considered sufficient to avoid excessive calculation costs and was used for the study. This mesh size corresponds to the meshes localized between an altitude of $z = 0$ and $z = 2H$. However, greater refinement was applied near the noise barrier walls and the road because of the strong gradients that can occur in these areas. This mesh size resulted in a total of 2.6 million meshes and an illustration of the meshes selected is provided in Figure 3. The meshing was done using the unstructured grid generator *snappyHexMesh* available with OpenFOAM.

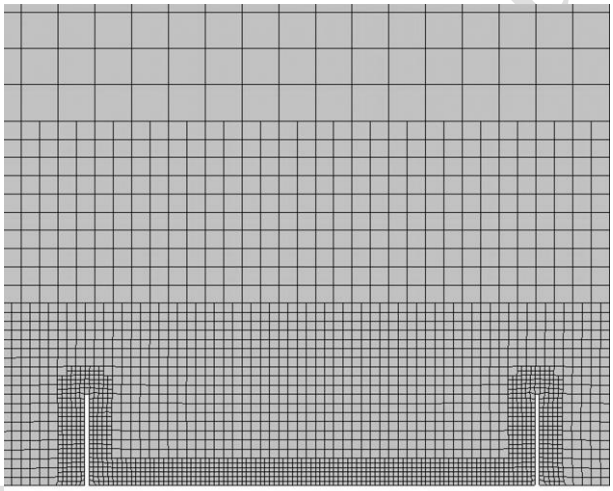

Fig.3. Grid selected for computation.

Several simulations were performed to study the combined effects of wind speed and thermal effects on the concentration reduction rate behind the barriers. All the simulations performed with their specific conditions (U_H and ΔT) and their corresponding Richardson numbers are given in Table 3. Each of these conditions was simulated twice to obtain results with and without noise barriers to calculate the concentration reduction rates. A total of 64 simulations were carried out including:

- 24 simulations for the neutral case (6 simulations for each of the three turbulent Schmidt numbers considered to assess their impact on the concentration reduction rates and 6 supplementary simulations for a non-perpendicular case);

DOI : 10.1016/j.jweia.2020.104160

- 20 simulations for the stable cases;
- 20 simulations for the unstable cases.

All the results were extracted at the center of the computational domain along $y/H = 0$ with $x/H = 0$ corresponding to the end of the downwind noise barrier wall.

Table 3. Summary of the simulations performed with wind velocity and thermal conditions ($\Delta T = T_H - T_w$) and their corresponding Richardson numbers.

U_H [m/s] / Ri [-]	1.18	1.96	3.15	5.51	7.87
0	ΔT = 0 K		ΔT = 0 K	ΔT = 0 K	
0.06				ΔT = 10 K	
0.17			ΔT = 10 K	ΔT = 30 K	ΔT = 62 K
0.33		ΔT = 7.5 K	ΔT = 19.5 K		
0.50		ΔT = 11.5 K	ΔT = 29.5 K		
1.20	ΔT = 10 K	ΔT = 27.5 K			
-0.06				ΔT = -10 K	
-0.17			ΔT = -10 K	ΔT = -30 K	ΔT = -62 K
-0.50		ΔT = -11.5 K	ΔT = -29.5 K		
-0.75		ΔT = -17.5 K	ΔT = -44.5 K		
-1.20	ΔT = -10 K		ΔT = -71 K		

Finally, the turbulent Schmidt number (Sc_t) is a dimensionless number found in air pollution CFD to consider the effect of turbulent diffusivity. However, this number is widely spread between 0.2 and 1.3, depending on the situation studied, and can significantly change the results in terms of concentration (Tominaga and Stathopoulos, 2007). To assess the effect of this parameter on noise barrier studies, three Sc_t were considered: 0.3, 0.7 and 1.1.

3.3. Model validation

The numerical model was compared against the experimental data proposed by Cui et al. (2016) because they provided results on both velocity and the concentration field for a complex 3D situation. Indeed, the experiment setup consists of two buildings with the downwind building being higher than the upwind building. A gas is released at the top of the upwind building and the ground between the two buildings is heated to simulate several atmospheric stabilities and heat exchanges. The downwind building is opened and closed by two windows to simulate indoor/outdoor pollutant exchanges.

DOI : 10.1016/j.jweia.2020.104160

Fig. 4 shows the comparison between the experimental data and the numerical model used in this study for an unstable case where Ri = -1.22 ($U_{free\ stream}$ = 0.7 m/s and ΔT = -135 °C) and for a vertical profile localized between the two buildings. These results are presented in a dimensionless form that can be found in the paper of Cui et al. (2016). The results show good agreement between the numerical model and the experimental data on both velocity and concentration profiles, with a mean difference of 6% between the experimental and numerical concentration profiles. The numerical model is therefore capable of accurately reproducing velocity and concentration profiles in a 3D case with a high thermal gradient. According to these results, the numerical model was considered validated for the purpose of this study.

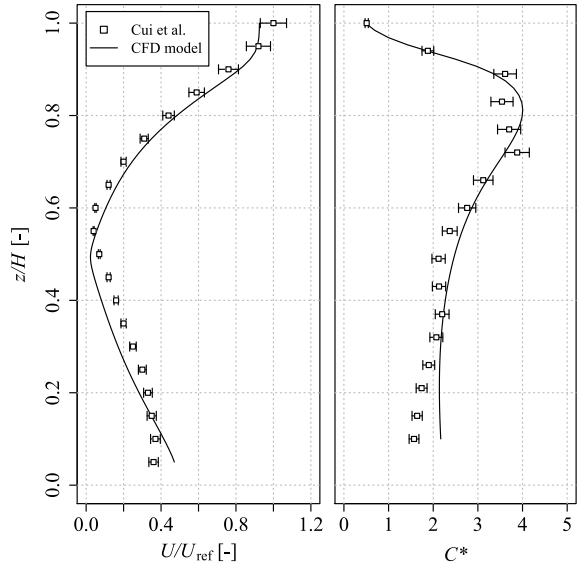

Fig.4. Vertical distribution of dimensionless velocity and concentration for Ri = -1.22 given by Cui *et al.* for the wind tunnel measurements (Cui et al., 2016), and comparison with the CFD model used for this study with Sc_t = 0.25.

4. Results

4.1. Study without thermal effects

4.1.1. Turbulent Schmidt number sensitivity

The evolution of the *CRR* behind the barriers for the three Sc_t considered and for four altitudes (z = 0.25H, 0.50H, 0.75H and 1.00H) are presented in Fig. 5 as a function of the dimensionless distance from the downwind noise barrier x/H, with z = 0.25H the pedestrian level corresponding particularly to the size of a child (1.25 m). The results show considerable variability for the concentration reduction rate as a function of the turbulent Schmidt number and no general trend can be observed. Indeed, while for Sc_t = 1.1 and z = 0.25H the *CRR* is

DOI : 10.1016/j.jweia.2020.104160

globally higher than for other turbulent Schmidt numbers, for the three other altitudes the *CRR* is not globally higher. Additionally, while the *CRR* is globally lower with $Sc_t = 0.3$ and $z = 0.25H$, this observation is no longer true for the other altitudes. Moreover, the turbulent Schmidt number has also an impact on the distance after the barriers were there is a positive impact of the noise barriers (*CRR* > 0), this distance being higher for higher Sc_t.

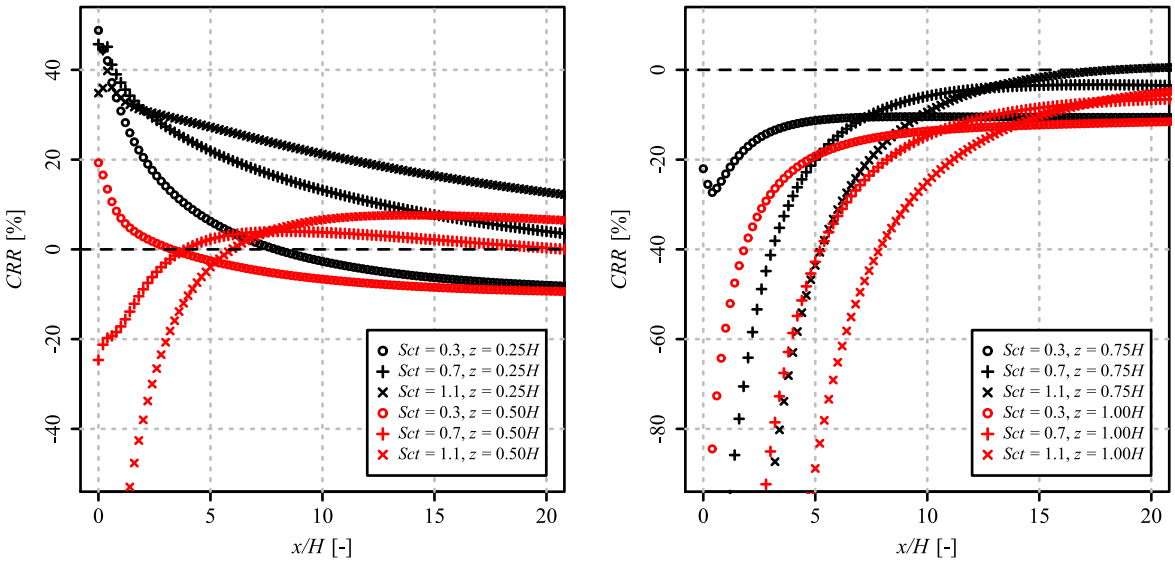

Fig.5. Evolution of the concentration reduction rate behind the downwind wall as a function of Sc_t and for several altitudes with the same wind profile (U_H = 1.18 m/s).

According to these results, it is important to state that the turbulent Schmidt number is also a very sensitive parameter when studying the impacts of noise barriers and its choice should be considered carefully, especially when performing quantitative studies. For the rest of this paper, and since no information or studies to determine the best turbulent Schmidt number for noise barrier studies are available an intermediate turbulent Schmidt number of 0.7 is used, as in Tominaga and Stathopoulos (2017), and the results are presented qualitatively rather than quantitatively.

4.1.2. Impact of wind speed and wind direction on the CRR in neutral atmosphere

The impact of wind speed and wind direction on the concentration reduction rate was first studied in neutral atmosphere, thus, considering only forced convection (i.e. convection due to the wind).

Fig. 6 shows the evolution of the pollutant concentrations behind the barriers for the cases with and without barriers (A) and the corresponding concentration reduction rates (B) as a function of the wind speed at $z = 0.25H$. According to Fig. 6 (A), regardless of the wind speed and for

DOI : 10.1016/j.jweia.2020.104160

$z = 0.25H$, pollutant concentrations were generally higher without the noise barrier than with it. Additionally, concentrations changed inversely with wind speed, leading to lower concentrations for higher wind speeds. The concentrations were thus different as a function of this parameter. However, as depicted in Fig. 6 (B), the *CRR* is the same whatever the wind speed considered and this is also true for the other altitudes considered ($z = 0.5H$, $0.75H$ and $1.00H$). This result is linked to the fact that, for a given wind direction and without thermal stratification, the concentration was inversely proportional to the wind velocity (Schatzmann and Leitl, 2011). Thus, since the concentration evolved in the same way with wind speed both with and without noise barriers, the *CRR* remained unchanged for a given wind direction under neutral conditions.

The effects of the wind direction under neutral conditions were also investigated and the results are presented in Fig. 7 for a perpendicular wind (90°) and a wind oriented at 60°. Fig 7 (A) shows that for the 60° case, the concentrations are lower with the noise barriers and higher without the noise barriers compared to the perpendicular case. This inevitably leads to a lower *CRR* for the perpendicular case, as shown in Fig. 7 (B) for $z = 0.25H$ and $z = 0.75H$. The same result was obtained for $z = 0.50H$ and $z = 1.00H$. Therefore, the *CRR* are higher for oblique wind directions.

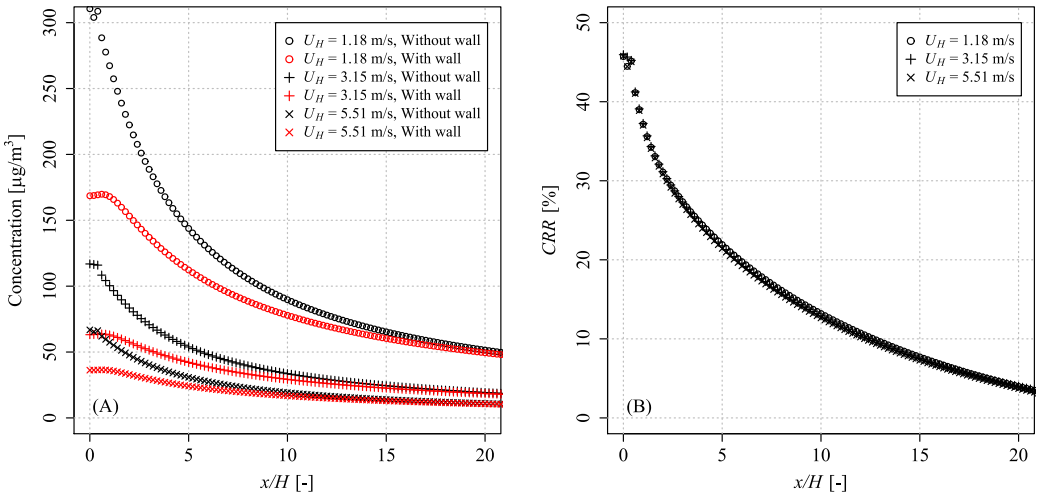

Fig.6. Evolution of the concentrations with and without noise barriers (A) and the concentration reduction rates (B) as a function of wind speed for a perpendicular wind direction at $z = 0.25H$.

DOI : 10.1016/j.jweia.2020.104160

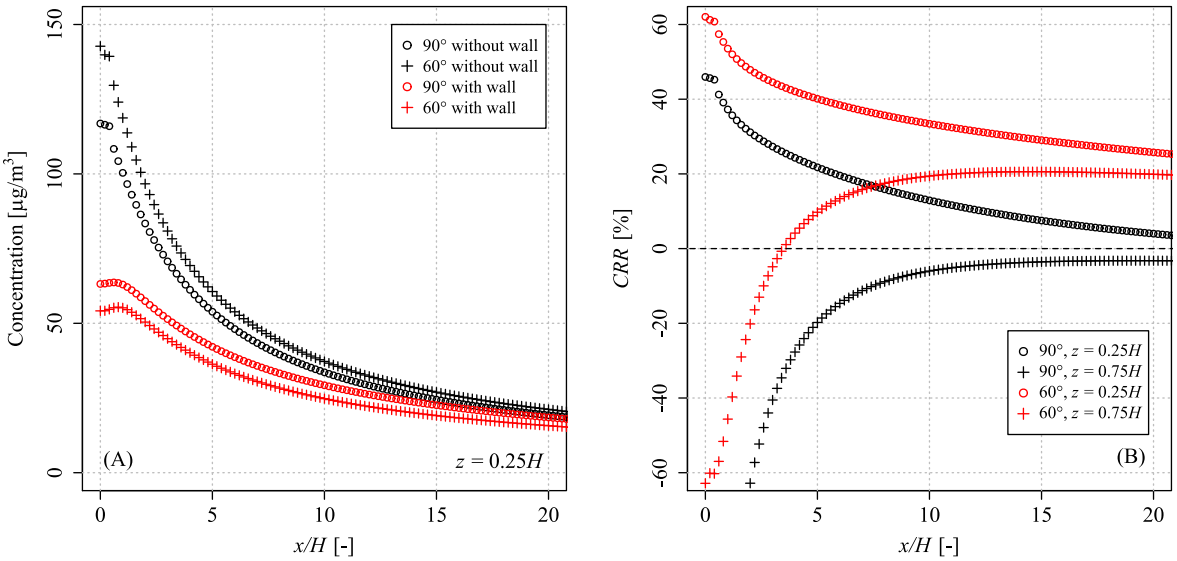

Fig.7. Evolution of the concentrations with and without noise barriers (A) and the concentration reduction rates (B) as a function of the wind direction and for a given wind speed (U_H = 3.15 m/s).

According to the previous results, when studying the CRR behind noise barriers for neutral cases, it is necessary to study only one wind speed for each wind direction. Moreover, if the minimal *CRR* is assessed, the study can be reduced to only one direction. Indeed, the perpendicular direction leads to the lowest *CRR* while the non-perpendicular directions lead to higher *CRR*.

4.2. Study with thermal effects

4.2.1. Evolution of the CRR as a function of the atmospheric stability

The concentration reduction rate was then studied considering mixed convection: forced convection induced by wind speed and natural convection induced by thermal stratifications. The *CRR* was therefore studied as a function of the Richardson number which includes wind speed (U_H) and thermal variations (ΔT).

The first results are presented in Fig. 8 for three different Richardson numbers: (A) Ri = 0.17 corresponding to a stable atmosphere; (B) Ri = 0 corresponding to a neutral atmosphere; and (C) Ri = -0.17 corresponding to a slightly unstable atmosphere, for the same wind conditions (perpendicular wind with U_H = 3.15 m/s). Thus, ΔT is the only variable here. For the three cases considered, the concentration is highest directly behind the barriers (x = 0 m), just above them (h = 5 m) and generally decreases as the distance from the barrier increases or the height

DOI : 10.1016/j.jweia.2020.104160

decreases. However, the concentrations are different depending on the case. Indeed, the concentrations are lowest for the stable case (A) and highest for the slightly unstable case (C). The neutral case (B) leads to intermediate results but closer to the unstable one. For a given wind speed and direction, thermal effects therefore have a high impact on the concentration behind the barriers and seem to have a greater impact for $\Delta T > 0$ than for $\Delta T < 0$.

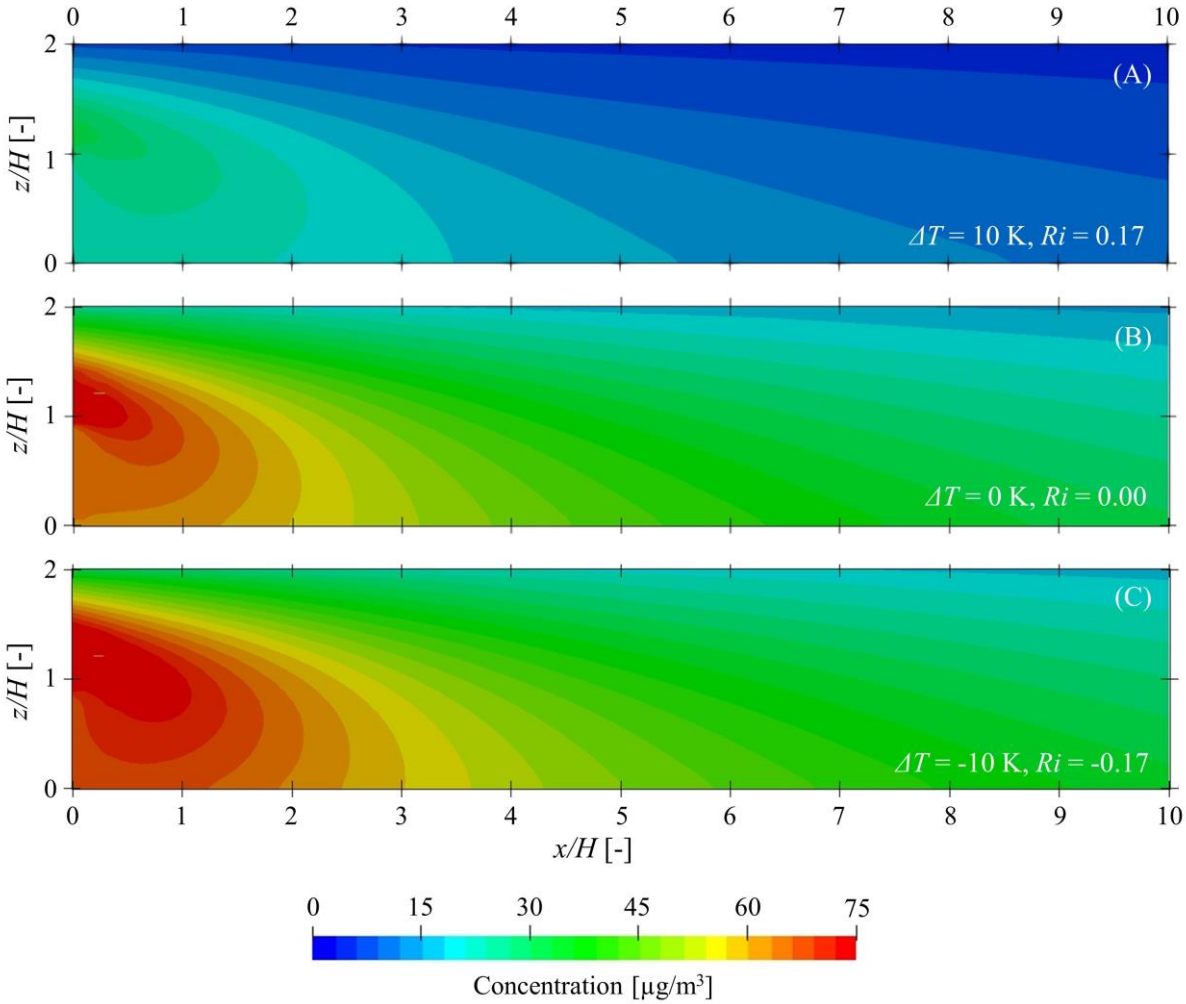

Fig.8. Evolution of the concentration behind the downwind barrier as a function of the temperature variation in the same wind conditions (perpendicular wind, U_H = 3.15 m/s).

The evolution of the *CRR* as a function of the distance from the downwind barrier was studied for several atmospheric stabilities by changing both the wind speed (U_H) and the thermal variation (ΔT). The results for *Ri* = -1.20, -0.17, -0.06, 0.00, 0.06, 0.17 and 1.20 are given in Fig. 9 for $z = 0.25H$ (A), $0.50H$ (B), $0.75H$ (C) and $1.00H$ (D). Further results are presented in Fig. 9 (E) and correspond to the *CRR* averaged over *z* for *z* ranging from 0 to 5 m giving global information along the height of the noise barriers.

DOI : 10.1016/j.jweia.2020.104160

As can be seen in Fig. 9, the evolution of the *CRR* follow the same trends. Indeed, for all the altitudes considered and also for the *CRR* averaged over $z = H$, the results for the neutral case are bounded by the results for the stable cases and the unstable cases: the unstable cases lead to lower *CRRs* compared to the neutral case, with the lowest *CRR* being obtained for the highest unstability level (Ri = -1.20). On the contrary, the stable cases lead to higher *CRRs* with the highest *CRR* being obtained for the highest stability level (Ri = 1.20). However, the evolution of the *CRR* according to the level of stability or unstability is not equivalent between the two cases. Indeed, whereas the results are different for the three unstable cases presented in Fig. 9, the *CRR* for the two highest stable cases (Ri = 0.17 and Ri = 1.20) are very similar. Furthermore, the *CRR* changes more quickly as a function of the Richardson number for the stable cases than for the unstable cases, which is consistent with the previous results discussed in relation with Fig. 8. Thus, atmospheric stability has an impact on the *CRR*, leading to higher *CRRs* for stable cases ($Ri > 0$), quickly reaching maximum values, while lower *CRRs* are obtained for unstable cases ($Ri < 0$) and no maximum values were reached for the Richardson numbers considered in this study.

Fig. 9 also shows that the *CRR* not only depends on the distance from the barriers but also on their height. For a given atmospheric stability, the *CRR* decreases with height and can reach negative values corresponding to an increase in pollutant concentration due to the barriers. These observations are related to the heights at which the plumes spread in both configurations, with and without the barriers. Indeed, without the noise barriers the plume spreads along the ground, leading to lower concentrations at $z = H$, while with the noise barriers the plume spreads from the top of the barriers and the concentrations are generally lower at ground level compared to the case without barriers.

DOI : 10.1016/j.jweia.2020.104160

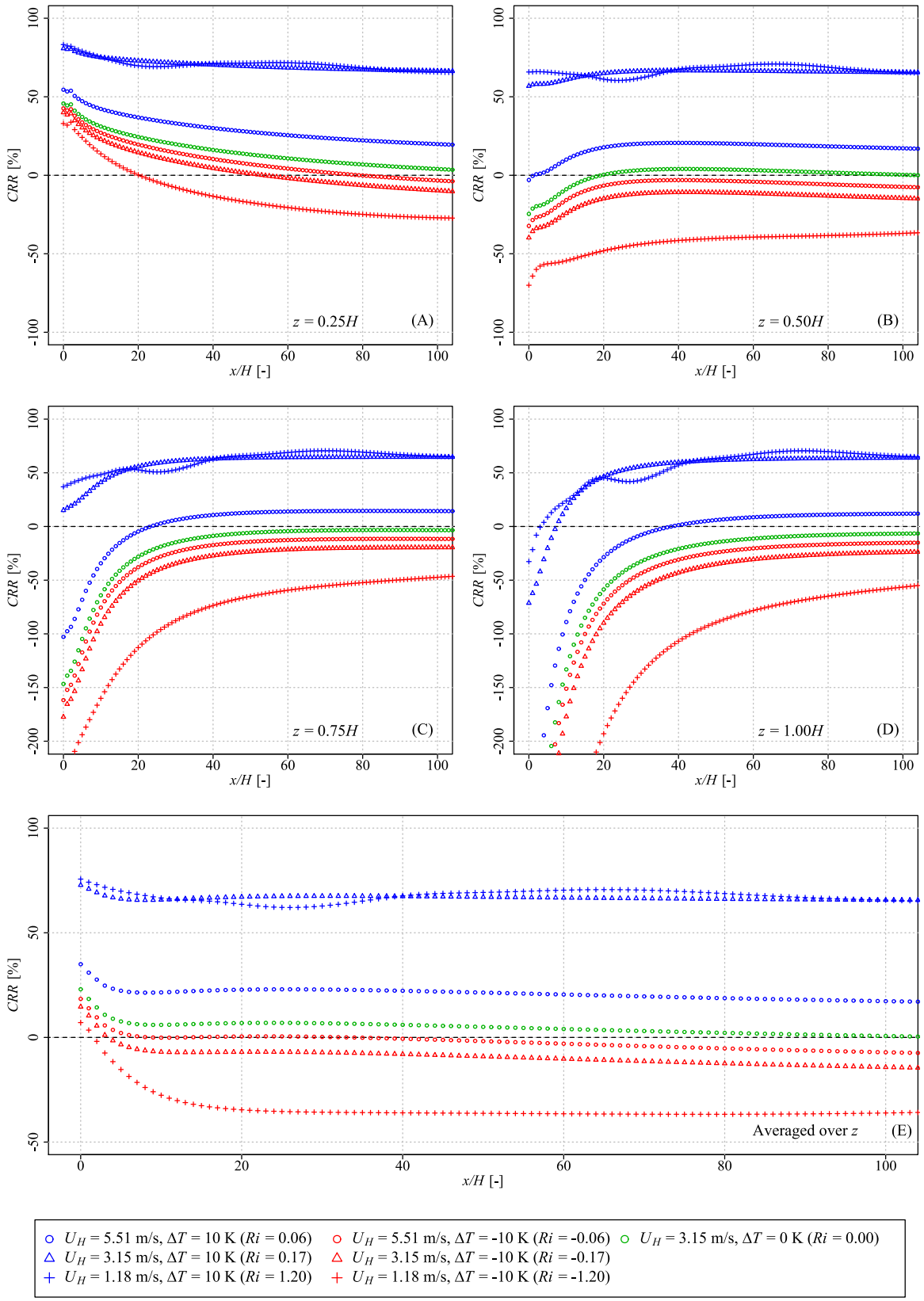

Fig.9. Evolution of the concentration reduction rates for 4 given altitudes (A—D) and averaged over the noise barrier height (E) as a function of the distance from the downwind barrier and for several Richardson numbers.

DOI : 10.1016/j.jweia.2020.104160

4.2.2. Conservation of the CRR with the Richardson number

It has been shown previously that the concentration reduction rate for a given wind direction is constant when considering only forced convection (neutral atmosphere) due to an inversely proportional link between the pollutant concentrations and the wind speed. However, this link is no longer valid when considering both forced and natural convection. The question was then to assess if the *CRR* is still constant for stable and unstable cases. To answer this question, several simulations were performed for numerous Richardson numbers but with distinct couples of wind speed and thermal variations. The Richardson numbers considered were Ri = -1.20, -0.75, -0.50, -0.17, -0.06, 0.00, 0.06, 0.17, 0.33, 0.50 and 1.50.

Fig. 10 (A) shows the evolution of the *CRR* for three couples of U_H and ΔT giving Ri = -0.17 (slightly unstable atmosphere) while Fig. 10 (B) shows the evolution of the *CRR* for two couples giving Ri = 0.50 (stable atmosphere). According to Fig. 10 (A), the *CRR* can be constant for a given Ri. Indeed, with Ri = -0.17, while the pollutant concentrations are not the same for the three couples of U_H and ΔT considered, the *CRR* is quasi-constant (± 3%). However, this observation is not true for all the Richardson numbers according to Fig. 10 (B), which shows that for Ri = 0.50 the *CRRs* are significatively different for the two couples of U_H and ΔT considered. Thus, the *CRR* can be constant for a given Ri but this is not generalizable.

The Richardson numbers for which the *CRR* can be considered constant were assessed and the results are presented in Fig. 11. The results show that, for a Ri ranging from -0.50 to 0.17, the variation over the *CRR* is less than 3% and the *CRR* can be considered as constant for a given Ri. For Richardson numbers outside this range, the variation over the *CRR* for a given Ri can reach 15% for a Ri ranging from -0.75 to -0.5 and 30% for a Ri ranging from -0.75 to -1.20 and from 0.17 to 1.20. According to these results, for a given Ri ranging from -0.50 to 0.17, a unique couple of U_H and ΔT must be considered when assessing the concentration reduction rates behind noise barriers in non-neutral cases.

DOI : 10.1016/j.jweia.2020.104160

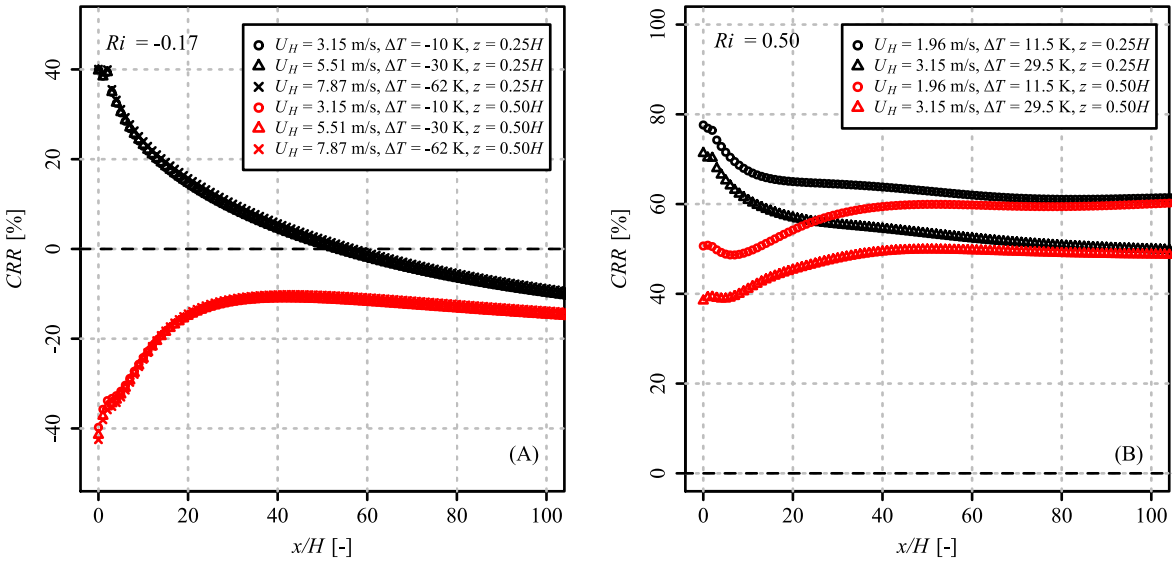

Fig.10. Evolution of the concentration reduction rate for Ri = -0.17 (A) and Ri = 0.50 (B) as a function of wind speed (U_H) and thermal variation (ΔT) at z = 0.25H and z = 0.50H.

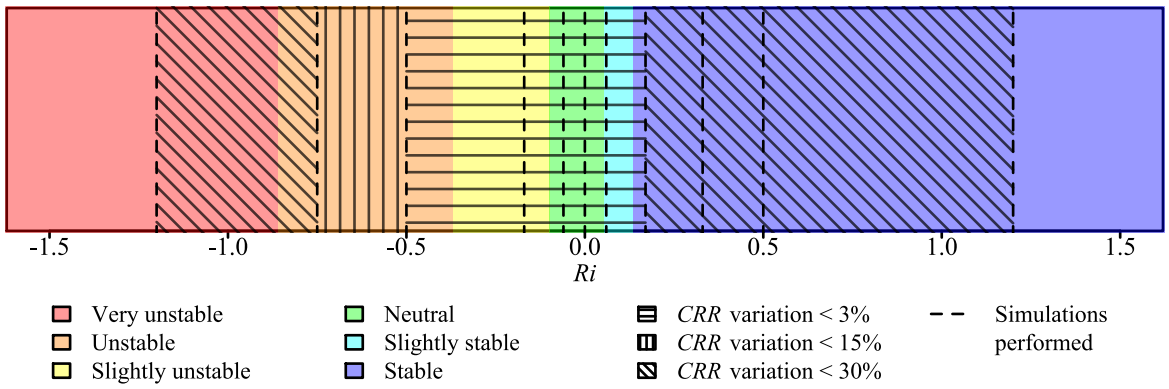

Fig.11. Conservation of the concentration reduction rate with the Richardson number.

5. Discussion

This study provides better understanding of how noise barriers can reduce air pollution and how this reduction can vary with wind conditions and atmospheric stability. Additional work can be done to further improve this understanding and is discussed below, as is the relevance of these results.

This study considered only one noise barrier configuration, with two walls of the same height placed on either side of a heavy-traffic road. Further studies could be performed to verify if the results obtained for this configuration are generalizable, for example for noise barriers with only one upwind or downwind wall and also with a combination of solid and vegetative barriers,

DOI : 10.1016/j.jweia.2020.104160

but also in presence of buildings before and after the barriers. Additionally, the height of $z = 0.25H$ (1.25 m) was considered to study the evolution of the *CRR* at the pedestrian level, which corresponds to the size of a child. The results were not provided for the size of adult people ($z = 0.35H$ = 1.75 m). However, results at this height can be approximated using both results at $z = 0.25H$ and $z = 0.50H$, for example by the means of a linear interpolation such as given in equation (12).

$$CRR_{0.35H} = 0.6 \times CRR_{0.25H} + 0.4 \times CRR_{0.50H} \qquad (12)$$

where $CRR_{0.35H}$ is the *CRR* at $z = 0.35H$, $CRR_{0.25H}$ is the *CRR* at $z = 0.25H$ and $CRR_{0.50H}$ is the *CRR* at $z = 0.50H$.

As shown in this paper, the turbulent Schmidt number has a different impact on the *CRR* depending on the location. There is no specific trend in the vicinity of the noise barrier. Indeed, there is an increase in the *CRR* when Sc_t increases at the height of the noise barrier while at ground level little variations are found. However, farther from the noise barrier, trends can be identified: the *CRR* systematically increases with increasing Sc_t, whatever the height considered.

It was shown that for a given *Ri* ranging from -0.50 to 0.17, variations over the *CRR* are negligible. Moreover, the evolution of the *CRR* as a function of distance from the downwind barrier seemed to follow the same trends, as the curves appear the same. Thus, it may be possible to find relationships between the *CRR* and the Richardson number in the range -0.50 to 0.17. If such relationships can be found, it will allow estimating all the *CRRs* in this *Ri* range by performing only one simulation, or with only one in-field measurement.

Finally, according to the results of this study, further studies can be simplified. Indeed, for future studies in neutral atmosphere (without thermal variations), they could be reduced to only wind direction and noise barrier configuration studies when assessing the evolution of the *CRR*. For studies including mixed convection (with thermal variations), for a *Ri* ranging from -0.50 to 0.17, only one couple of wind speed and thermal variation is needed to assess the evolution of the *CRR*.

DOI : 10.1016/j.jweia.2020.104160

6. Conclusion

The effects of wind speed and atmospheric stability on the concentration reduction rate (*CRR*) of air pollutants induced by noise barriers were studied with a validated CFD model. This study considered both numerous wind conditions (wind speed and direction) and thermal variations, leading to different atmospheric stabilities ranging from very unstable cases to stable cases. Several CFD simulations were carried out and the main conclusions are as follows:

(a) When no thermal variations are considered, i.e. for a neutral atmosphere, the evolution of the *CRR* depends only on the wind direction: wind speed changes the pollutant concentrations behind the barriers but this parameter does not change the *CRR*.

(b) A non-perpendicular wind direction leads to higher pollutant concentrations without noise barriers and lower concentrations with the barriers compared to perpendicular cases. The *CRRs* are therefore minimal for a perpendicular wind.

(c) The *CRR* decreases with height due to the different locations of the plume for the two cases with and without noise barriers. The global *CRR* decreases with distance from the downwind barrier.

(d) The *CRR* obtained with forced convection (neutral atmosphere) is bounded by the *CRR* obtained with mixed convection (stable and unstable atmospheres): higher *CRRs* are obtained in stable conditions ($Ri > 0$) while lower *CRRs* are obtained in unstable conditions ($Ri < 0$).

(e) For a given Richardson number ranging from -0.50 to 0.17, the *CRR* is constant with a variation of less than 3%. For numbers outside this range the variation increases to 15% for a *Ri* ranging from -0.75 to -0.5 and 30% for a *Ri* ranging from -1.20 to -0.75 and from 0.17 to 1.20.

Finally, these results give insights to researchers and civil engineers to better understand variations of air pollutant concentrations behind noise barriers, for example for carrying out further assessment studies on the impact of noise barriers on the reduction of air pollution, and for in-field monitoring campaigns.

Acknowledgments

We would like to thank the ANRT (Association Nationale de la Recherche et de la Technologie) for their support.

DOI : 10.1016/j.jweia.2020.104160

References

Amini, S., Ahangar, F.E., Heist, D.K., Perry, S.G., Venkatram, A., 2018. Modeling dispersion of emissions from depressed roadways. Atmospheric Environment 186, 189–197. https://doi.org/10.1016/j.atmosenv.2018.04.058

Anderson, J.O., Thundiyil, J.G., Stolbach, A., 2012. Clearing the Air: A Review of the Effects of Particulate Matter Air Pollution on Human Health. J. Med. Toxicol. 8, 166–175. https://doi.org/10.1007/s13181-011-0203-1

Baldauf, R., Thoma, E., Khlystov, A., Isakov, V., Bowker, G., Long, T., Snow, R., 2008. Impacts of noise barriers on near-road air quality. Atmospheric Environment 6. https://doi.org/10.1016/j.atmosenv.2008.05.051

Baldauf, R.W., Isakov, V., Deshmukh, P., Venkatram, A., Yang, B., Zhang, K.M., 2016. Influence of solid noise barriers on near-road and on-road air quality. Atmospheric Environment 129, 265–276. https://doi.org/10.1016/j.atmosenv.2016.01.025

Bowker, G.E., Baldauf, R., Isakov, V., Khlystov, A., Petersen, W., 2007. The effects of roadside structures on the transport and dispersion of ultrafine particles from highways. Atmospheric Environment 41, 8128–8139. https://doi.org/10.1016/j.atmosenv.2007.06.064

Brechler, J., Fuka, V., 2014. Impact of Noise Barriers on Air-Pollution Dispersion. NS 06, 377–386. https://doi.org/10.4236/ns.2014.66038

Chen, H., Kwong, J.C., Copes, R., Tu, K., Villeneuve, P.J., van Donkelaar, A., Hystad, P., Martin, R.V., Murray, B.J., Jessiman, B., Wilton, A.S., Kopp, A., Burnett, R.T., 2017. Living near major roads and the incidence of dementia, Parkinson's disease, and multiple sclerosis: a population-based cohort study. The Lancet 389, 718–726. https://doi.org/10.1016/S0140-6736(16)32399-6

Cui, P.-Y., Li, Z., Tao, W.-Q., 2016. Buoyancy flows and pollutant dispersion through different scale urban areas: CFD simulations and wind-tunnel measurements. Building and Environment 104, 76–91. https://doi.org/10.1016/j.buildenv.2016.04.028

DOI : 10.1016/j.jweia.2020.104160

Enayati Ahangar, F., Heist, D., Perry, S., Venkatram, A., 2017. Reduction of air pollution levels downwind of a road with an upwind noise barrier. Atmospheric Environment 155, 1–10. https://doi.org/10.1016/j.atmosenv.2017.02.001

European Commission, 2013. Proposal for a Directive of the European Parliament and of the Council on the reduction of national emissions of certain atmospheric pollutants and amending Directive 2003/35/EC. European Commission (EC), Brussels, Belgium.

Finkelstein, M.M., Jerrett, M., Sears, M.R., 2004. Traffic Air Pollution and Mortality Rate Advancement Periods. American Journal of Epidemiology 160, 173–177. https://doi.org/10.1093/aje/kwh181

Finn, D., Clawson, K.L., Carter, R.G., Rich, J.D., Eckman, R.M., Perry, S.G., Isakov, V., Heist, D.K., 2010. Tracer studies to characterize the effects of roadside noise barriers on near-road pollutant dispersion under varying atmospheric stability conditions. Atmospheric Environment 11. https://doi.org/10.1016/j.atmosenv.2009.10.012

Franke, J., Hellsten, A., Schlünzen, H., Carissimo, B., 2007. Best practice guideline for the CFD simulation of flows in the urban environment. COST Action 732.

Gong, L., Wang, X., 2018. Numerical Study of Noise Barriers' Side Edge Effects on Pollutant Dispersion near Roadside under Various Thermal Stability Conditions. Fluids 3, 105. https://doi.org/10.3390/fluids3040105

Hagler, G.S.W., Lin, M.-Y., Khlystov, A., Baldauf, R.W., Isakov, V., Faircloth, J., Jackson, L.E., 2012. Field investigation of roadside vegetative and structural barrier impact on near-road ultrafine particle concentrations under a variety of wind conditions. Science of The Total Environment 419, 7–15. https://doi.org/10.1016/j.scitotenv.2011.12.002

Hagler, G.S.W., Tang, W., Freeman, M.J., Heist, D.K., Perry, S.G., Vette, A.F., 2011. Model evaluation of roadside barrier impact on near-road air pollution. Atmospheric Environment 45, 2522–2530. https://doi.org/10.1016/j.atmosenv.2011.02.030

Heist, D.K., Perry, S.G., Brixey, L., 2009. A wind tunnel study of the effect of roadway configurations on the dispersion of traffic-related pollution. Atmospheric Environment 43(32). https://doi.org/10.1016/j.atmosenv.2009.06.034

DOI : 10.1016/j.jweia.2020.104160

528 Kagawa, J., 1985. Evaluation of biological significance of nitrogen oxides exposure. Tokai J.
529 Exp. Clin. Med. 10, 348–353.

530 Kim, K.-H., Kabir, E., Kabir, S., 2015. A review on the human health impact of airborne
531 particulate matter. Environment International 74, 136–143.
532 https://doi.org/10.1016/j.envint.2014.10.005

533 Koutsourakis, N., Bartzis, J.G., Markatos, N.C., 2012. Evaluation of Reynolds stress, k-ε and
534 RNG k-ε turbulence models in street canyon flows using various experimental datasets.
535 Environmental Fluid Mechanics 12, 379–403. https://doi.org/10.1007/s10652-012-
536 9240-9

537 Lee, E.S., Ranasinghe, D.R., Ahangar, F.E., Amini, S., Mara, S., Choi, W., Paulson, S., Zhu,
538 Y., 2018. Field evaluation of vegetation and noise barriers for mitigation of near-
539 freeway air pollution under variable wind conditions. Atmospheric Environment 175,
540 92–99. https://doi.org/10.1016/j.atmosenv.2017.11.060

541 Ning, Z., Hudda, N., Daher, N., Kam, W., Herner, J., Kozawa, K., Mara, S., Sioutas, C., 2010.
542 Impact of roadside noise barriers on particle size distributions and pollutants
543 concentrations near freeways. Atmospheric Environment 44, 3118–3127.
544 https://doi.org/10.1016/j.atmosenv.2010.05.033

545 Papageorgakis, G.C., Assanis, D.N., 1999. COMPARISON OF LINEAR AND NONLINEAR
546 RNG-BASED k-epsilon MODELS FOR INCOMPRESSIBLE TURBULENT FLOWS.
547 Numerical Heat Transfer, Part B: Fundamentals 35, 1–22.
548 https://doi.org/10.1080/104077999275983

549 Petters, A., von Klot, S., Heier, M., Trentinaglia, I., 2004. Exposure to Traffic and the Onset of
550 Myocardial Infarction. The New England Journal of Medicine 351, 1721–1730.
551 https://doi.org/10.1056/NEJMoa040203

552 Richards, P.J., Hoxey, R.P., 1993. Appropriate boundary conditions for computational wind
553 engineering models using the k-E turbulence model 9.

554 Richards, P.J., Norris, S.E., 2011. Appropriate boundary conditions for computational wind
555 engineering models revisited. Journal of Wind Engineering and Industrial
556 Aerodynamics 99, 257–266. https://doi.org/10.1016/j.jweia.2010.12.008

DOI : 10.1016/j.jweia.2020.104160

557 Roache, P.J., 1994. Perspective: A Method for Uniform Reporting of Grid Refinement Studies.
558 Journal of Fluids Engineering 116, 405. https://doi.org/10.1115/1.2910291

559 Schatzmann, M., Leitl, B., 2011. Issues with validation of urban flow and dispersion CFD
560 models. Journal of Wind Engineering and Industrial Aerodynamics 99, 169–186.
561 https://doi.org/10.1016/j.jweia.2011.01.005

562 Schulte, N., Snyder, M., Isakov, V., Heist, D., Venkatram, A., 2014. Effects of solid barriers
563 on dispersion of roadway emissions. Atmospheric Environment 97, 286–295.
564 https://doi.org/10.1016/j.atmosenv.2014.08.026

565 Tominaga, Y., Stathopoulos, T., 2017. Steady and unsteady RANS simulations of pollutant
566 dispersion around isolated cubical buildings: Effect of large-scale fluctuations on the
567 concentration field. Journal of Wind Engineering and Industrial Aerodynamics 165, 23–
568 33. https://doi.org/10.1016/j.jweia.2017.02.001

569 Tominaga, Y., Stathopoulos, T., 2007. Turbulent Schmidt numbers for CFD analysis with
570 various types of flowfield. Atmospheric Environment 41, 8091–8099.
571 https://doi.org/10.1016/j.atmosenv.2007.06.054

572 United Nations, Department of Economic and Social Affairs, Population Division, 2019. World
573 Urbanization Prospects: The 2018 Revision (ST/ESA/SER.A/420). New York: United
574 Nations.

575 Wang, S., Wang, X., 2019. Modeling and Analysis of the Effects of Noise Barrier Shape and
576 Inflow Conditions on Highway Automobiles Emission Dispersion. Fluids 4, 151.
577 https://doi.org/10.3390/fluids4030151

578 Woodward, J.L., 1998. Estimating the flammable mass of a vapor cloud, A CCPS concept book.
579 Center for Chemical Process Safety of the American Institute of Chemical Engineers,
580 New York, N.Y.

581 Yakhot, V., Orszag, S.A., Thangam, S., Gatski, T.B., Speziale, C.G., 1992. Development of
582 turbulence models for shear flows by a double expansion technique. Physics of Fluids
583 A: Fluid Dynamics 4, 1510–1520. https://doi.org/10.1063/1.858424

584